A Fluid Dynamics Calculation of Sputtering from a Cylindrical Thermal Spike.

M. M. Jakas*[(a)], E. M. Bringa[(b)], and R.E. Johnson[(b)]
[(a)] *Departamento de Física Fundamental y Experimental, Universidad de La Laguna, 38201 La Laguna, Tenerife, Spain*
and,
[(b)] *Engineering Physics, University of Virginia. Charlottesville, VA 22903, U.S.A.*
(August 13, 2013)

The sputtering yield, Y, from a cylindrical thermal spike is calculated using a two dimensional fluid dynamics model which includes the transport of energy, momentum and mass. The results show that the high pressure built-up within the spike causes the hot core to perform a rapid expansion both laterally and upwards. This expansion appears to play a significant role in the sputtering process. It is responsible for the ejection of mass from the surface and causes fast cooling of the cascade. The competition between these effects accounts for the nearly linear dependence of Y with the deposited energy per unit depth that was observed in recent Molecular Dynamics simulations. Based on this we describe the conditions for attaining a linear yield at high excitation densities and give a simple model for this yield.

PACS numbers: 79.20.Rf, 47.40.Nm, 83.85.Pt

I. INTRODUCTION

The ejection of atoms from the surface of a solid during ion irradiation is well documented both experimentally and theoretically[1]. This phenomenon, known as sputtering, is due to the energy transferred to the atoms in the target by the incident ion. This produces a cascade which can cause some atoms to overcome the surface's attractive barrier and escape to vacuum.

In previous theoretical work the mean number of ejected atoms per incoming ion, or sputtering yield Y, is related to the energy deposited the ion per unit thickness at the surface of the target F_D, as $Y \propto F_D^n$. The value of the power n depends on the type of collision cascade produced by the ion, namely linear and non-linear cascades. For linear cascades, when the density of moving atoms N_{mov} within the cascade is small compared to normal density N_0, one has $n = 1$[2,3], whereas in the non-linear case $N_{mov} \sim N_0$ theoretical work predicted that n must be greater than one[4,5]. These results are so firmly established that the consensus among workers in the field is that $n > 1$ and non-linear cascades are to some extent synonymous[6]. Similar results have been found for sputtering in response to electronic energy deposited in a solid[7], but here we refer to work on collision cascade sputtering.

Recent Molecular Dynamics (MD) studies[8,9], however, cast doubt on this relationship. According to these papers, purposely prepared non-linear cascades can give rise to sputtering yields which depend linearly on F_D (see figures 2-4). Further evidence is found in Ref.[10]. After modifying the standard thermal spike theory (STST) to include the transport of mass, the sputtering yields so calculated appeared to be much closer to a linear function of F_D than to the F_D^2 predicted by the STST.

Although the results in Ref.[10] show the importance of having a target which can change its specific volume as a fluid, it is not a full fluid dynamics calculation. Since the target was assumed to be infinite, the sputtering yields had to be calculated in the same manner as in the STST. That is, an expression for the evaporation rate was used that was borrowed from the kinetic theory, and the sputtering yields were obtained by integrating it along a plane representing an otherwise non-existent surface. Further, the transport was only radial, but the MD calculations showed the importance of energy transport along the track.

In order to circumvent such a difficulty, our previous calculations are extended to a target which, in addition to being compressible, has a solid-vacuum interface. To this end, the target density, velocity and internal energy are all assumed to vary with time in a manner which is described by the fluid dynamics equations. Consequently, sputtering emerges naturally, as that part of the target that succeeds in escaping from the condensed to the gaseous phase.

The aim of this paper is to show the most relevant aspects of those calculations, from the underlying mathematics to the results and implications of the proposed model. Although the present calculations can be applied to a variety of ion-induced thermal spike cases, we have purposely limited ourselves to the cases contained in previous MD simulations[8,9]. Therefore, the results in this paper are intended for cylindrical thermal spikes. In Section II we introduce the fluid dynamics equations as well as the various expressions used along the present calculations. Results and discussions are presented in Section III. Finally, the conclusions and suggestions for further studies are presented in Section IV.

II. THEORY

We assume that the target is a continuous medium with cylindrical symmetry, and it is completely characterized by its atomic number density N, velocity $\mathbf{v}$, and internal energy ϵ (per atom) defined as,

$$\epsilon = U + \frac{3}{2}k_B T, \tag{2.1}$$

where k_B is the Boltzmann's coefficient, T the temperature and U is the potential energy per atom. It must be noted that by using the equation above the heat capacity at constant volume, C_V , is assumed to be that of a dilute gas, i.e. $3k_B/2$. This approximation however is fairly acceptable for the purpose in this paper, since as shown in Ref.[11], the quadratic dependence of Y with F_D does not appear to be connected to C_V . Moreover U is obtained from the expression[10]

$$U = (N_0 M c_o^2/\mu)\ (N/N_0)^{\nu+\mu-1}\ \left[\frac{1}{\nu+\mu-1} - \frac{(N/N_0)^2}{\nu+\mu+1}\right] , \tag{2.2}$$

where M is the mass of the target atom, c_o is the speed of sound at $T = 0K$, and N_0 is the normal atomic number density. μ and ν are two numerical constants which, as we explained in Ref.[10], are not independent. Thus we set $\mu = 2$, then $\nu = \sqrt{1 + Mc_0^2/U_0}$, U_0 being the potential energy at normal density, i.e. $U_0 = -U(N_0)$.

Using the same notation as in Ref.[12], we write the fluid dynamics equations as follows

$$\frac{\partial N}{\partial t} = -\frac{\partial (v_k N)}{\partial x_k} , \tag{2.3}$$

$$\frac{\partial v_i}{\partial t} = -v_k \frac{\partial v_i}{\partial x_k} - \frac{1}{NM}\left(\frac{\partial p}{\partial x_i} + \frac{\partial \sigma'_{ik}}{\partial x_k}\right) \tag{2.4}$$

$$\frac{\partial \epsilon}{\partial t} = -v_k \frac{\partial \epsilon}{\partial x_k} + \frac{1}{N}\left(Q_{con} + Q_{vis} - p\frac{\partial v_k}{\partial x_k}\right) , \tag{2.5}$$

where the subscripts stand for the r and z coordinates, p is the pressure and σ'_{ik} is the viscosity tensor[12] defined as,

$$\sigma'_{ik} = \eta\left(\frac{\partial v_i}{\partial x_k} + \frac{\partial v_k}{\partial x_i}\right) , \tag{2.6}$$

where η is the *dynamic viscosity* coefficient and Q_{con} and Q_{vis} account for the heat produced by thermal conduction and viscosity per unit volume and time, namely

$$Q_{con} = \nabla\left(\kappa_T \nabla T\right) , \tag{2.7}$$

where κ_T is the thermal conductivity and,

$$Q_{vis} = \sigma'_{ik}\frac{\partial v_i}{\partial x_k} . \tag{2.8}$$

The heat conduction coefficient is replaced by that in Ref.[5]

$$\kappa_T = \frac{25}{32}\frac{k_B}{\pi a^2}\sqrt{\frac{k_B T}{\pi M}} , \tag{2.9}$$

where $\pi a^2 = 1.151\text{Å}^2$. This form was used in order to compare results and because there seems to be no reason for using a more "realistic" one since, as shown in Ref.[11], κ_T and the quadratic dependence of the sputtering yield appear not to be connected.

Making use of the fact that, for dilute gases, η and κ_T are related through the equation $\eta = \kappa_T M/(3k_B)$, we thus introduce the dimensionless viscosity coefficient

$$\eta^* = 3k_B\eta/(M\kappa_T) . \tag{2.10}$$

Similarly, the pressure p is assumed to be a function of both temperature and density. Here, we follow the approximation in Ref.[13] and split p into two terms

$$p = p_T + p_C , \tag{2.11}$$

where the *thermal pressure* p_T can be obtained from the expression

$$p_T = \lambda\ N k_B T, \tag{2.12}$$

λ being a numerical constant. The so called *crystal pressure* p_C can be obtained from the potential energy Eq.(2.2) using the equation[13]

$$p_C = N^2\frac{\partial U}{\partial N} . \tag{2.13}$$

For computational purposes, Eqs. (2.3-2.5) are applied to a finite system, which is defined by inequalities $0 \le r \le R_{max}$ and $0 \le z \le z_{bot}$ (see figure 1). Furthermore, the top wall, i.e. $z = 0$, is assumed to be made of a perfectly absorbent material, whereas the boundary at the bottom is perfectly closed as far as to the exchange of mass, momentum and energy is concerned. The lateral wall can be made either closed, like the bottom surface, or partially open. That is, closed to mass transport but open to energy and momentum exchange. Results in this paper were obtained using the latter option. Otherwise, in the case of a large deposited energy, one would need an exceedingly large target to minimize the effects of energy and momentum reflections. A more detailed description of this program will be published elsewhere[14].

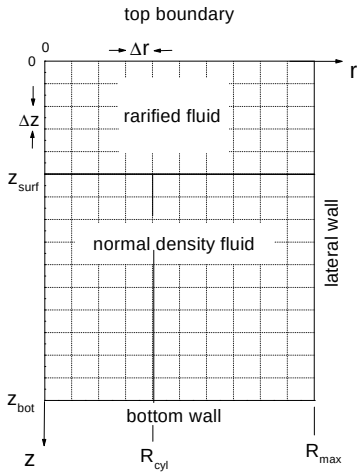

Figure 1: Frame of reference and grid. /Jakas et al./

FIG. 1. Sketch illustrating the frame of reference and grid utilized in the present calculations. At t=0 the "fluid" occupies the region defined by inequalities $z_{surf} < z < z_{bot}$ and $0 < R < R_{max}$, and the hot spike is confined to a cylinder of radius R_{cyl}.

At $t = 0$ the target is within a range of z defined by inequality ($z \geq z_{surf}$). For numerical reasons however, we assume that the region that would normally be a vacuum is filled with a low-density fluid, i.e. $N_{min} = 10^{-3} \times N_0$. Exchange of energy, momentum and matter is forbidden in this fluid, as well as in any other piece of a fluid with density lower than $N_{\min}$. The possible net flux of matter is continuously checked along the fluid, and the restrictions above are relaxed as soon as an element of the fluid would have its density increased above N_{min}.

To energize the spike, all atoms within a cylinder of radius R_{cyl} are given an energy E_{exc} above their initial energy, $\epsilon_0 = -U_0 + (3/2)k_B T_0$, where T_0 is the background temperature, often assumed to be 10 K. These are the initial conditions used in a number of the MD simulations[8,9], again allowing direct comparison with the results here. The initial conditions for Eqs.(2.3-2.5) thus become,

$$v_{r,z}(0,r,z) = 0 \ ,$$

$$N(0,r,z) = \begin{cases} N_0 & \text{if} \quad z \geq z_{surf} \\ N_{min} & \text{otherwise} \end{cases} \tag{2.14}$$

$$\epsilon(0,r,z) = \begin{cases} E_{exc} + \epsilon_0 & \text{if } \ r \leq R_{cyl} \text{ and } z \geq z_{surf} \\ U(N_{min}) + (3/2)k_B T_0 & \text{if } 0 \leq z < z_{surf} \\ \epsilon_0 & \text{otherwise} \end{cases}$$

With the assumptions above, the deposited energy becomes,

$$F_D = \pi R_{cyl}^2 N_0 E_{exc} \ .$$

As is customary, in solving the fluid dynamics equations the functions N, $\mathbf{v}$ and ϵ are defined over a discrete set of $NR \times NZ$ points, whose mesh size is determined by Δr and Δz (See figure 1 and Table I). A compromise has to be made about target size since a large target implies a fairly large system of coupled equations with fairly long running times. Whereas too small a target gives rise to boundary effects that would make calculations meaningless. Similarly, in choosing z_{surf} one has to take into account that during ejection not all the matter that crosses the surface will be ejected. Therefore, the distance between the initial surface and the top wall should be large enough to not "collect" matter that, otherwise, would not be ejected. Finally, the piece of matter representing the target must be thick enough. The condensed phase is assumed to be 10σ thick, which means that $z_{surf} \approx 10\sigma$ and $z_{bot} \approx 20\sigma$. $NR = 40$ and $NZ = 20$ were found to be adequate for all the cases studied in this paper.

When integrating the fluid dynamics equations (2.3,2.4,2.5) from t =0 to t_f, the total flux of matter passing through the top boundary is also calculated. In this way the sputtering yield is obtained as a function of time, $Y(t)$. This is used to verify if t_f was long enough so that no matter remains within the system that may significantly contribute to the sputtering yield. We use the $Y(t)$'s for $t < t_f$ to extrapolate $Y(t)$ to infinity, i.e. $Y_\infty = \lim_{t_f \to \infty} Y(t_f)$. Only runs for which $Y_\infty - Y(t_f) \approx 0.1 Y_\infty$ are accepted. Normally, t_f ranging from 10 up to 50 ps are required.

Since calculations in this paper are meant to be compared with those in MD simulations, which often use Lennard-Jones (LJ) potentials, the various parameters characterizing our system correspond to those of Argon (see Table I). M=40u and U_0=0.08eV have become standard parameters[8,9] although the LJ calculations fully scale with U_0 and M. Therefore, the results apply to a broader set of materials as shown also using a Morse potential[15]. Consistent with this, for most cases we used $\Delta r = \Delta z = \sigma$, where σ is the LJ distance. However, as several approximations were introduced, we cannot ensure that the fluid in our calculations accurately describes the potentials used in the MD simulations. Similarly, we do not want to leave this section without mentioning that although the fluid representing the target is assumed to be compressible, Eq.(2.6) looks the same as that of an incompressible fluid because the Stokes' condition is assumed to hold.

TABLE I. Value of the parameters used in the present calculations.

Property	Symbol	Value
Atomic mass	M	40.0 u.m.a.
Atomic number density	N_0	0.026 at/Å^3
Speed of sound	c_0	17 Å/ps
Binding energy	U_0	0.08 eV
Lennard-Jones distance	σ	3.405 Å

III. RESULTS AND DISCUSSIONS

We calculated the sputtering yield for different values of λ, η^* and the speed of sound c_o, and the results are depicted in figures 2 to 4. We observe that in all the cases the yield increases with increasing excitation energy E_{exc}. Similarly, $E_{exc} \approx U_0$ is an effective threshold for ejection for the initial radius used, since the yields rapidly decrease for E_{exc} comparable to or less than U_0. Whereas the MD requires varying potential types to obtain different material properties, here we do this by directly varying the material properties. In this manner the relationship between different materials can be described.

We observe that λ has a great influence on the sputtering yield. The larger the λ the greater the yield. λ=4 appears to reproduce MD-simulations quite well, whereas λ=2 and 1 underestimate the yields at small excitation energies. These results are, to some extent, easy to understand: with all other parameters remaining the same, as λ becomes larger the thermal pressure build up within the spike increases and more ejection is expected.

It must be noted, however, that the total energy, c.f. Eq.(2.1), does not depend on λ. Increasing λ only increases the thermal pressure and speeds up the conversion of thermal motion into directed kinetic energy. Therefore, thermal conductivity has less time to take energy away from the spike and the ejection of matter increases.

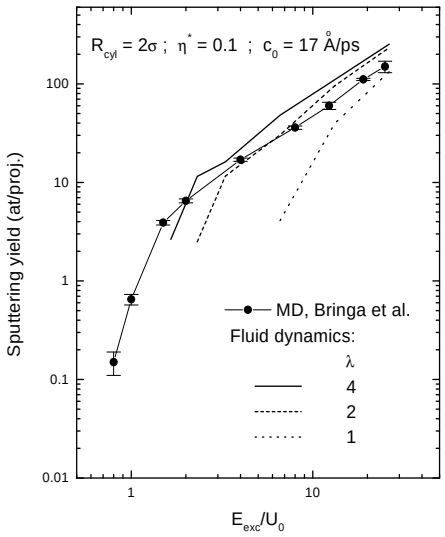

Figure 2: Sputtering yield for different thermal pressure coefficient (λ). /Jakas et al./

FIG. 2. Sputtering yield as a function of the excitation energy and different values of parameter λ.

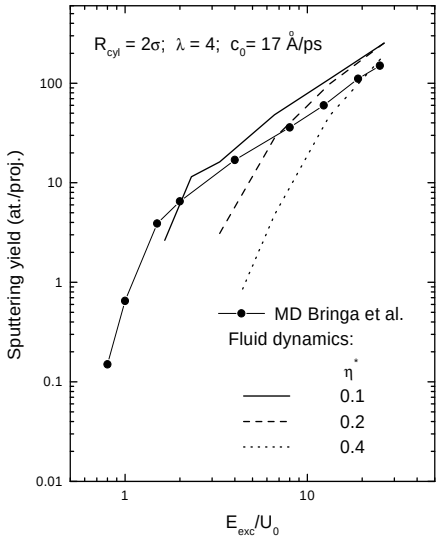

Figure 3: Sputtering yield for different viscosity coefficient (η*). /Jakas et al./

FIG. 3. Sputtering yield as a function of the excitation energy and different values of viscosity coefficient η^*.

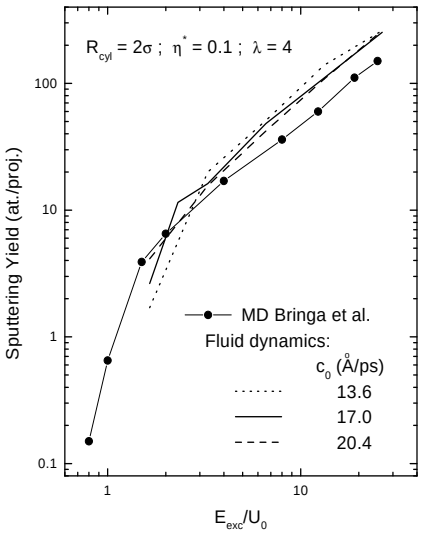

Figure 4: Sputtering yield for different speed of sound. /Jakas et al./

FIG. 4. Sputtering yield as a function of the excitation energy and different values of the speed of sound c_0.

The role played by the viscosity on the sputtering yield is illustrated in figure 3. For the cases studied here, we observed that viscosity has a negative influence on the ejection process, as yields are seen to get smaller with

an increase of the viscosity coefficient. At small excitation energies the viscosity appears to play a major role. Furthermore, calculations using $\eta^* = 0.1$ produced a good agreement with MD-simulations while those with $\eta^* = 0.2$ and 0.4 resulted in significantly smaller yields. The fact that the best agreement with MD-simulations corresponds to calculations with $\eta^* = 0.1$ is not unexpected since η^*-values of approximately that order have been calculated for a Lennard-Jones fluid[16].

Finally, modifying the speed of sound does not produce a significant change in the sputtering yield. Figure 4 shows results for the speed of sound both above and below its normal value. The change in the sputtering yield is very small compared that produced by changing either the viscosity coefficient or the thermal pressure coefficient λ. We observe that, for high excitation energies, an increase in the speed of sound leads to a slightly greater yield, and that such a trend is reversed as E_{exc}/U_0 becomes smaller than 3.

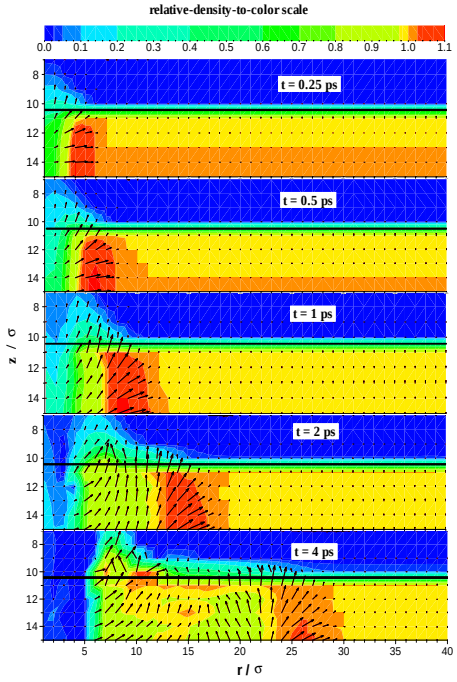

Fig 5: Density and mass-flux. /Jakas et al./

FIG. 5. These plots illustrate the density and mass-flux vectors at different times for a spike with dE/dX=4eV/Å, λ=4, η^*=0.1, c_0=17 Å/ps and $R_{cyl} = 2\sigma$. The scale used for translating from relative density (N/N_0) into colors is shown up in the figure. Note that the scale is non-linear, as more colors are used at both small densities and around N/N_0=1. Furthermore, due to interpolation in the plotting software, details of the order of the grid size, or smaller, might not be accurately copied. The horizontal line denotes the initial position of the surface.

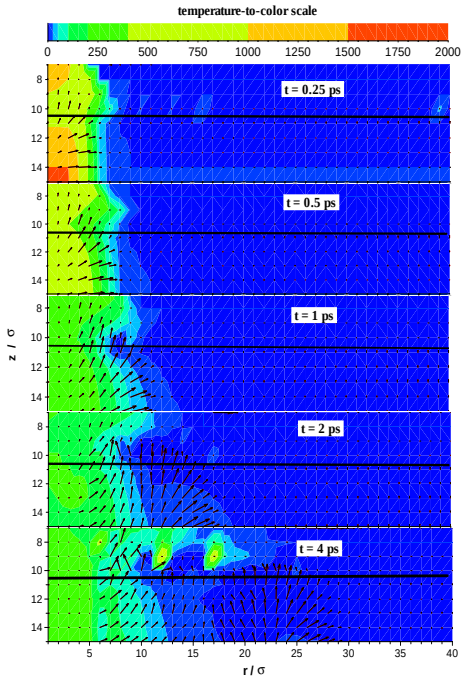

Fig 6: Temperature and mass-flux. /Jakas et al./

FIG. 6. Temperature and mass-flux vectors at different times within the fluid for the spike described in caption 5. The scale used for color vs. temperature appears up in the figure.

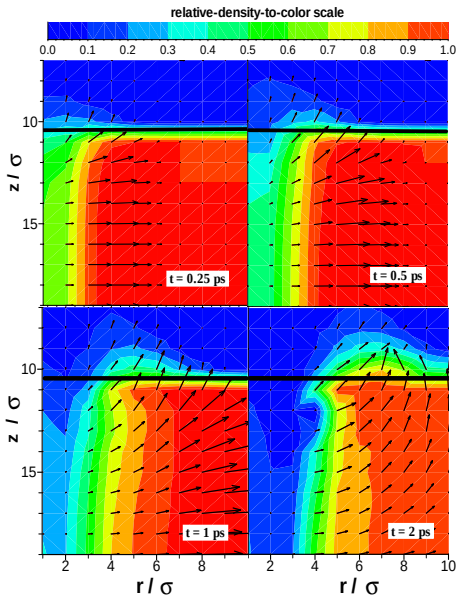

Fig 7: Details of the ejection process. /Jakas et al./

FIG. 7. Close-ups of plots in figure 5 illustrating in more details the dynamics of the fluid within the "core" of the spike and near the surface.

As we mentioned in the introduction, the most interesting result in this paper is our ability to explore the material parameters that lead to the near linearity exhibited in the yield in our MD calculations even though the sputtering is a non-linear process. By exploring the parameter space we can better explain that phenomenon and assess its relevance. Our calculated yields in figures 2-4 clearly show that a linear region is attained for $E_{exc} > U_0$ using a set of materials parameters. Therefore, non-linear sputtering does not necessarily imply non-linear yields. From these figures, it also appears that linearity is approached at higher energy densities than those studied here for other materials parameters. Below we describe this phenomenon.

To understand the change in the dependence of the yield with increasing excitation density for fixed R_{cyl}, we analyzed the time-evolution of the spike paying particular attention to those aspects of the energy and momentum transport that are related to the ejection of matter. To this end, in figures 5-6 we have plotted the density, the mass-flux vector and temperature in the fluid at different times after the on-set of the spike. These cases correspond to a deposited energy of 4 eV/Å, $\lambda = 4$, η^*=0.1, c_0=17 Å/ps and R_{cyl}=2σ; and, in the three figures, the initial surface is located at 10σ, i.e. $z_{surf} = 10\sigma$.

One readily observes that the temperature within the spike drops below 500 K in approximately 1 ps, and that the fluid immediately surrounding the spike hardly reaches temperatures higher than, say, 100 K. This is in agreement with our MD results and our earlier fluid dynamics calculations[10]. These studies already showed that, due to the quick, adiabatic expansion of the fluid, the temperature of the spike decreases much more rapidly than it would due to thermal conduction. In addition, for times greater than 1 ps the thermal energy appears to be converted into an elastic wave (seen as red in Fig. 5) that travels in the radial direction at approximately the speed of sound. The reader must be aware of the non-linear scale used in Fig. 5 where colors were purposely chosen so as to change rapidly around both N_0 and at low density. Due to this, even the rather small relaxation of the surface density appears as a yellow stripe, which extends to the right of the spike and gets thicker with increasing time. These figures show us that the whole process would be better described as an "explosion" rather than a smooth, thermally diffusive release of energy as proposed in the STST[5].

Note that, in contrast to material further away from the surface, the fluid that is near the surface and within the spike, appears to follow a spherical, rather than a cylindrical expansion. That is, if one interpolates the mass-flux vector and figures out the streamlines of the fluid, then, one can readily see that near the open boundary of the spike, they seem to radiate out from a point located on the spike axis somewhere below the surface. In order to understand this, one has to realize that the momentum acquired by any particle within the fluid results from the fast, though small, displacements of the lateral and top boundaries which takes place at an earlier stage of the aforementioned explosion.

The forces produced by such displacements propagate at the speed of sound which, within the hot spike, is faster than c_0[17]. Therefore, by the time all the fluid within the spike has been set into motion, i.e. $t = R_{cyl}/c$ after the onset of the spike, a particle at (r, z) with $0 \leq z \leq R_{cyl}$ and $0 \leq r \leq R_{cyl}$ will have acquired a velocity that is proportional to the time it has been exposed to such forces, namely $v_r \propto r$ and $v_z \propto -(R_{cyl} - z)$. Therefore, as $v_z/v_r \approx -(R_{cyl} - z)/r$ this particle will appear as moving away from a point located exactly on the axis at R_{cyl} below the surface. By the same token, any particle at a depth greater than R_{cyl} within the spike, will remain unaware of the presence of the surface and its velocity will be directed along the radial direction (see figure 7). With increasing time our description above will become less and less accurate. However, as the forces acting within the spike take the largest values during the earliest stage of the "explosion", the velocities achieved by the fluid during that time essentially determine the subsequent dynamics of the spike.

Another aspect of the velocity field which deserves attention is that around the rim, on the cold side of the spike. Contrary to what happens deep in the target, where the cold side is compressed and subsequently displaced along the radial direction, the rim is partially wiped out. This not only adds more matter to sputtering per se, but also clears the way for further ejection as it widens the sputtering radius, or the radius from within which particles are ejected.

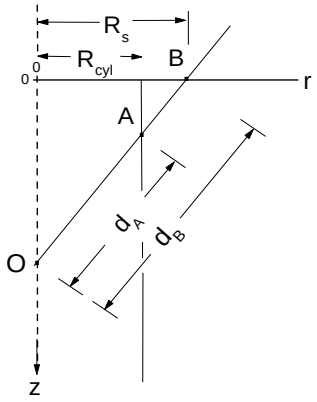

Figure 8: The sputtering radius. /Jakas et al./

FIG. 8. Schematics used to obtain the sputtering radius.

From this simple picture one can readily calculate the

sputtering radius. To this end, we define the excess energy as the total energy per particle relative to the bottom of the potential well, i.e. $e = \epsilon + \frac{1}{2}Mv^2 + U_0$. If one assumes that the elastic wave in the upper part of the spike propagates isentropically along the streamlines, one may write

$$e_A/d_A^2 = e_B/d_B^2 \ , \tag{3.1}$$

where d_A and d_B are the distance from the center of the spherical expansion to points A and B, respectively (see figure 8); similarly, e_A and e_B are the corresponding excess energies. Therefore, as $e \geq U_0$ is a necessary condition for ejection, $e_A = E_{exc}$ and $R_{cyl}/d_A = R_B/d_B$, one can obtain the sputtering radius (R_s) as[18]

$$R_s \approx R_{cyl}\,(E_{exc}/U_0)^{1/2} \ , \tag{3.2}$$

Accordingly, the sputtering yield can be calculated as the amount of mass contained within a cone of height R_{cyl} and base radius R_s, i.e.

$$Y \approx \frac{\pi}{3} N R_{cyl}^3 \frac{E_{exc}}{U_0} \ , \tag{3.3}$$

In order to verify this simple expression, we calculate the sputtering yield for different spike radii. The results, that appear in figure 9, show that our fluid dynamics calculations compare fairly well with the MD yields, and that Eq.(3.3) accounts reasonably well for the yields at high-excitation energies. Discrepancies between MD and fluid dynamics at low excitation energies and for small spike radii do appear. A detailed analysis of such deviations was not carried out. As previously mentioned, the various quantities entering our model do not accurately account for the Lennard-Jones fluid in the MD simulations. In addition, having assumed the solid target is a fluid, effects arising from the crystalline structure and the atomic nature of the target can not be described. In the MD simulations focused collision sequences play an important role at carrying energy and momentum away from the spike, particularly for small spike radii. Finally, it is worth noticing that equation (3.3) predicts a linear dependence of the yield with the excitation or deposited energy. A result that was derived in Ref.[19] using a simple, intuitive model rather than well supported, rigorous calculation.

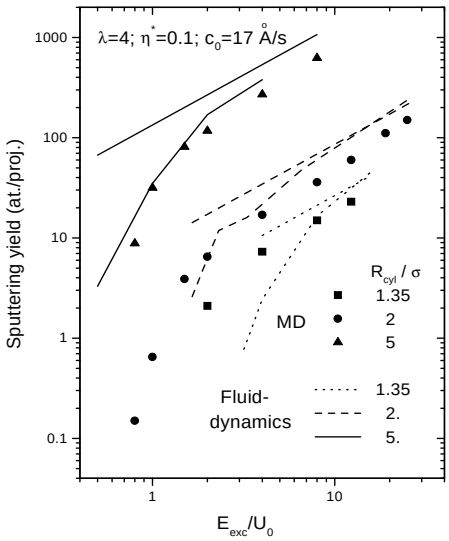

Figure 9: Yields for differents spike radii /Jakas et al./

FIG. 9. Sputtering yield for different spike radii. MD calculations appear as symbols whereas Hydrodynamics results are plotted as thick lines. Thin, straight lines show the sputtering yield obtained using Eq. (3.3).

Although we have chosen not to address to the problem of crater formation, it is worthwhile observing that late in our calculations craters do appear, and they are all surrounded by a rim several σ high (the reader is referred to Ref.[20] for additional information about crater formation). The hole left by the spike is normally greater than the initial radius of the hot core. It is formed as the result of the net displacement produced by the elastic wave along the radial direction. Near the edge of the hole, the radial momentum is less than it is in the material below. As a result, a kind of cantilever is formed which is pushed upwards by the fluid below. See the case of t=2 ps in figure 7. It is important to mention, however, that for E_{exc} smaller than, say U, then no hole is formed.

IV. CONCLUSIONS

Sputtering at relatively high excitation densities is an old but unsolved theoretical problem in ion solids interactions. Analytic diffusive thermal spike models are commonly used to interpret data at high excitation densities, although these models were never tested against more detailed calculations. In addition, there is a history of applying ideas from fluid dynamics to explain sputtering at high excitation density. These models are called by a number of names (gas flow[21], shock[19], pressure pulse[22] etc.) and attempt to account for the fact that sputtering at high excitation density does not occur on an atom by

atom basis. These models also require a more detailed theoretical justification.

Establishing a theoretical basis for sputtering models at high excitation density has been addressed recently by MD simulations using model materials and simplified descriptions of the initial conditions. It was shown that standard spike models break down at precisely those high excitation densities which they were intended to treat. In addition, a new sputtering regime was found. On increasing the energy density in the spike for fixed spike radius, the yield changed from a non-linear dependence on the excitation density to a linear dependence even though the ejection process clearly remained non-linear. This is contrary to the conventional wisdom and suggests saturation occurs in the sputtering. To examine this result we first showed that such a regime is never attained for any set of material properties using the diffusive thermal spike model[11]. Since the standard spike model involves solving only the energy equation, we then numerically integrated the full set of fluid equations for a 1D model of a cylindrical spike[10]. Differences with the MD result remained which we attributed to the lack of a surface. Here use a 2D fluid dynamics model with a surface to confirm that when the full set of equations is treated the MD result at high excitation density can be attained. Therefore, as pointed out earlier, the principal deficiency of the standard spike model is the assumption that the transport is diffusive.

We have calculated for the first time the sputtering yield from a cylindrical thermal spike by directly integrating the full 2D fluid-dynamics equations. The transport of mass and momentum are seen to play a significant role in the ejection process. Since the conversion of the thermal energy into kinetic/potential energy within the spike occurs very early, the ejection process at high energy densities is much more closely related to an "explosion" rather than to the thermal diffusion and evaporation models[5] typically used to describe sputtering at high energy densities. Comparisons with MD-simulations using appropriate material parameters, show that our fluid dynamics description can account for the main features of the cylindrical thermal spike. These calculations also confirm the MD result that transport along the cylindrical axis is as important as radial transport and, therefore, a 2D model is required. We show the reported nearly linear yield comes about because of the competition between pressurized ejection and the transport of energy away from the spike by the pressure pulse.

Using the evolution of the streamlines seen in these calculations we obtain a simple expression for the yield at high excitation density for a reasonable set of material parameters. Bringa and co-workers ([15],[23]) had shown that in this regime the yield could be written in the form, $Y \approx C[R_{cyl}/l]^m\{[dE/dx]_{eff}(l/U_0)\}^p$ where $[dE/dx]_{eff}$ is the energy deposited that ends up fueling the spike (here $\pi R_{cyl}^2 N E_{exc}$) and m and p are close to one. They gave $C \approx 0.18$ for an LJ solid, which also appeared to apply to results for other pair potentials[15]. Here we use a picture of the ejection attained from the 2D fluid dynamics model to establish the theoretical basis for the value of C. That is, the internal pressure in the spike determines a critical radius ($R_s \approx R_{cyl}(Eexc/Uo)^{1/2}$) and a depth $\sim R_{cyl}$, leading to the ejection of a conical volume of material $Y \approx \frac{1}{3} R_{cyl}\pi R_s^2 N$. This gives $C = \frac{1}{3}$, which is larger than the MD result. The difference is due in part to the fact that the material properties are not exactly those of the LJ solid and transport along crystal axes removes energy from the spike as discussed, however, all the principal features of the transport and ejection are the same. This new model resembles that of Yamamura and co-workers[19] but disagrees with the 'so-called' pressure pulse model used for molecular materials[22].

Several points need further investigation. The formation of craters at normal incidence is a topical problem that can be addressed by the model developed here. Further, the connection between the sputtering yield and the time used to heat the spike needs to be studied. In this paper, as in most of the MD simulations, we assumed it to be negligibly small. This may be correct for spike formation by a collision cascade, but is known to fail for electronic sputtering of rare-gas solids[7]. Finally, it must be noted that the fluid dynamics description of the spike is a useful complement to MD. In the fluid model a broad range of material properties and types can be readily studied, whereas complicated potentials are needed in MD calculations of different materials. In fact it is seen in Figs 2-3 that the saturation leading to the linear regime is not simply dependent on the cohesive energy ($E_{exc} \approx U_0$) and the initial R_{cyl}, as found in the MD simulations using pair potentials, but also depends on the material parameters λ and η^*. In addition, local equilibrium chemistry, which can play an important role in many of the materials of interest to us, can be readily included in the fluid models. However, MD has the advantage that non-normal incidence can be treated easily, the state of the ejecta (clusters vs. atoms) can be studied, and non-equilibrium chemistry can be introduced. Therefore, a program in which complementary calculations using fluid dynamics and MD simulations is underway. Here we have shown that a new linear sputtering regime is seen in both models and we have developed a simple analytic model for the yield at normal incidence.

ACKNOWLEDGMENTS

Part of this work was carried out during a visit performed by one of the authors (MMJ) to the School of Engineering and Applied Science, University of Virginia. Financial aid from the Astronomy and Chemistry Divisions of the National Science Foundation (U.S.A.) and the Consejería de Eduación, Cultura y Deportes del Gobierno Autónomo de Canarias (Spain) are acknowledged.

* Corresponding author. e-mail: *mmateo@ull.es*.

[1] See for example C.T. Reimann. Mat.-fys. Medd **43**, Det. Kong. Dan. Vid. Selsk. 351 (1993) and references therein.
[2] M. W. Thompson. Phil.Mag. **18**, 377 (1968).
[3] P. Sigmund. Phys.Rev. **184**, 383 (1969).
[4] R.E. Johnson and R. Evatt. Radiation Effects, **52**, 187 (1980).
[5] P. Sigmund and C. Claussen. J. Appl. Phys. **52**(2), 990 (1981).
[6] H.H. Andersen. Phy.Rev.Letters **80**, 5433 (1999).
[7] R.E. Johnson and J. Schou Mat.-fys. Medd **43**, Det. Kong. Dan. Vid. Selsk. (1993).
[8] H.M. Urbassek, H. Kafemann and R.E. Johnson. Phys. Rev. **B 49**, 786 (1994-II).
[9] E.M. Bringa and R.E. Johnson. Nucl. Instr. Methods in Phys. Res. **B 152**, 167 (1999).
[10] M.M. Jakas and E.M. Bringa. Phys. Rev. **B 62**, 824 (2000).
[11] M.M. Jakas. Radiation Effects and Defects in Solids, **152**, 157 (2000).
[12] L.D.D. Landau. Fluids Mechanics 2nd Ed., Butterworth-Heinemann (1995).
[13] Yu. B. Zel'dovich and Yu. P. Raizer. Physics of shock waves. Academic Press (1969).
[14] M.M. Jakas. *In preparation.*
[15] E.M. Bringa, M.M. Jakas and R.E. Johnson. Nucl. Instr. Methods in Phys. Res. **B 164-165**, 762 (2000).
[16] J.O. Hisrchfelder, C.F. Curtiss and R.B. Bird in *Molecular Theory of Gases and Liquids* John Wiley & Sons, Inc. (1964).
[17] If the temperature of the spike is high, then, the speed of sound (c) is greater than c_0 since $c = (p/MN)^{1/2}$, therefore according to Eq.(2.11), $c = \left(\lambda k_B T + c_0^2\right)^{1/2}$.
[18] It must be noticed that, except for a numerical factor, Eq.(3.2) coincides with the *effective sputtering radius* derived by H.Urbassek and P.Sigmund [Appl.Phys. **A 33**, 19 (1984)] using a Gaussian thermal spike. As they were obtained using different models such an agreement appears to be a remarkable coincidence for which we have no feasible explanation.
[19] Y. Kitazoe, N. Hiraoka and Y. Yamamura. Surface Science **111**, 381-394 (1981).
[20] Z. Insepov, R. Manory, J. Matsuo and I. Yamada. Phys. Rev. **B 61**, 8744 (2000).
[21] H.M.Urbassek and J. Michl. Nucl. Instr. and Methods in Phys. Res. **B22**, 480 (1987).
[22] D. Fenyö and R.E. Johnson. Phys. Rev. **B 46**, 5090 (1992-I)
[23] E.M. Bringa, R.E.Johnson and M.M. Jakas. Phys. Rev. **B 60**, 15107 (1999)